

# A new binary decagonal Frank-Kasper quasicrystal phase

Johannes Roth\*

Institut für Theoretische und Angewandte Physik, Universität Stuttgart,  
Pfaffenwaldring 57, D-70550 Stuttgart, Germany

Christopher L. Henley

\*Laboratory of Atomic and Solid-State Physics, Cornell University,  
Ithaca, NY 14853-2501, USA

October 14, 2018

## Abstract

A structure model of atoms of two sizes, interacting with Lennard-Jones potentials and simulated by molecular dynamics, was observed to freeze into a decagonal quasicrystal dominated by Frank-Kasper coordination shells and closely related to the Henley-Elser model for icosahedral quasicrystals. Idealized structure models can be described as decorations of triangle-rectangle and rhombus tilings. Equilibrium properties of the idealized model have been determined by molecular dynamics simulations and a high stability of the model and a low jump rate of the atoms have also been observed.

PACS: 61.44.Br, 61.50.Ah, 61.43.Bn

preprint ITAP-3/96-1

## 1 Introduction

The well-studied quasicrystals fall essentially into two families, the Al-transition metal family exemplified by  $i(\text{AlPdMn})$  and the Frank-Kasper family (Frank and Kasper, 1958; Frank and Kasper, 1959; Shoemaker, Shoemaker and Wilson, 1957; Shoemaker and Shoemaker, 1988) exemplified by  $i(\text{AlCuLi})$ . Decagonal quasicrystals are known experimentally only in the first family, except for one claim (He, Yang and Ye, 1990).

Recently, three dimensional model systems have been found which, in simulations, freeze into a quasicrystal phase with Frank-Kasper local structure: a monatomic system with a special potential freezes into a dodecagonal quasicrystal (Dzugutov, 1993), and a system of large (L) and small (S) atoms with Lennard-Jones interactions freezes into an icosahedral phase (Roth, Schilling and Trebin, 1995), in fact a simplified version of the Henley-Elser structure model for  $i(\text{AlCuLi})$  and  $i(\text{AlZnMg})$  (Henley and Elser, 1986). Since Frank-Kasper systems are dominated by *sp* conduction electrons, it is believed that simple pair potentials (as used in these simulations) can offer a good approximation to the structure energy (Hausleitner and Hafner, 1992). The L and S atoms used by Roth et al. (1995) had single-well potentials where the ideal distances are non-additive ( $r_{LL} \approx r_{LS} \approx 1.15r_{SS}$ ).

This paper reports on a new *decagonal* Frank-Kasper phase which froze from the liquid in molecular dynamics simulations of a model system using practically the same potentials as Roth et al. (1995) (see Sec. 2). No realization of this structure in nature has been established (except conceivably in  $d(\text{FeNb})$ , as discussed in Sec. 6.4). However, in the absence of a *realistic* model system, a toy model system with an equilibrium quasicrystal phase can be quite useful. (To date, microscopically derived potentials for particular alloy systems have not been used in simulations of freezing from the melt (Mihalkovič, Zhu, Henley and Phillips, 1996b), but only for comparisons

of trial structures at zero temperature, in the Al-transition metal case (Phillips, Deng, Carlsson and Murray, 1991; Zou and Carlsson, 1994; Widom, Phillips, Zou and Carlsson, 1995; Widom and Phillips, 1993; Phillips and Widom, 1994; Mihalcovič, Zhu, Henley and Oxborrow, 1996; Mihalcovič et al. 1996b). Of course, there is some fundamental interest in the existence of any microscopic model of interacting atoms which has a quasicrystal equilibrium state. Furthermore, within such a model one can study the phonon/phason coupling, the energy changes and barriers corresponding to tile flips, the phason elastic constants with their temperature dependence, and can derive from microscopics an effective Hamiltonian in terms of tile-tile interactions (Mihalcovič et al. 1996a). In two dimensions, the “binary tiling” case (Lançon, Billard and Chaudhari, 1986; Widom, Strandburg and Swendsen, 1987) has served this purpose, but it has quite unrealistic bond radii, in contrast to our model potentials (which were in fact tailored to favor the i(AlCuLi) structure (Roth, Schilling and Trebin, 1990)).

The bulk of our paper presents an idealized decoration model which was constructed by abstracting the patterns observed in our simulations. The model has several variants, corresponding to closely related atomic structures, yet described by different tilings (See Sec. 3). Thus it exemplifies a system where an effective tile-tile Hamiltonian may select a less disordered subensemble of a random tiling ensemble (Jeong and Steinhardt, 1994). We have constructed the acceptance domains of a quasiperiodic version of our model (Sec. 4). Finally, by applying information from the ideal model, we adjusted the potentials so as to obtain a better-ordered structure after quenching (Sec. 5). In the concluding section, we have discussed how our model is related to others, and how realistically it extends beyond our small system size.

## 2 Initial Simulations

Our decagonal phase was first seen in a slow-cooling simulation of a binary liquid. (Further details about this simulation and other structures observed, as well as the motivation for our initial choice of parameters for the potential, can be found (Roth et al. 1995). The interaction is described by Lennard-Jones potentials

$$v_{\alpha\beta}(r) = 4\epsilon_{\alpha\beta} \left( \left( \frac{\sigma_{\alpha\beta}}{r} \right)^{12} - \left( \frac{\sigma_{\alpha\beta}}{r} \right)^6 \right) \quad (1)$$

The bond parameters  $\sigma_{\alpha\beta}$  are  $\sigma_{SS} = 1.05$ ,  $\sigma_{SL} = 1.23$ , and  $\sigma_{LL} = 1.21$ . These and all other simulation parameters are given in reduced or Lennard-Jones units, and are indicated by a star. The corresponding bond lengths are  $2^{1/6}\sigma_{\alpha\beta}$ . In overall outline, these distances are appropriate for a typical tetrahedrally-close-packed structure, in which the small atoms have icosahedral coordination shells and the large atoms have Frank-Kasper coordination shells with larger coordination number. (Frank-Kasper structures are by definition “tetrahedrally close-packed (tcp)”, meaning that neighboring atoms always form tetrahedra (Samson, 1968; Samson, 1969; Shoemaker et al. 1957; Frank and Kasper, 1958; Frank and Kasper, 1959). This is not strictly true in our model – or that of Henley and Elser (1986) – since there is a small number of non-tcp environments.)

The coupling constants were set to  $\epsilon_{SS} = \epsilon_{LL} = 0.656$  for same species and to  $\epsilon_{SL} = 1.312$  for different species, in order to prevent phase separations into monatomic domains. To save computation time we cut off the potential smoothly at  $r_c = 2.5\sigma_{SL}$ .

For the simulation we have modified the standard molecular dynamics method to allow us to control pressure and temperature as described by Evans and Morriss (1983). A constant cooling rate may be introduced by the method described by Lançon and Billard (1990). The equations of motion are integrated in a fourth-order Gear-predictor-corrector-algorithm (see for example Allen and Tildesley (1987)). The time increment  $\delta t^*$  is adjusted after testing for numerical stability. We find that  $\delta t^* = 0.00462$  is an appropriate value. For simplicity the masses of small and large atoms are set to unity.

Our simulation box is a cube containing 128 small (S) and 40 large (L) atoms. The initial positions are set with a random number generator, and then relaxed. The generated liquid is equilibrated at an initial temperature of about  $T^* = 1.0$ . At high cooling rates we observe a

transition from a supercooled liquid to a glass at about  $T^* = 0.5$ . If the cooling rate is lowered to  $T^*/t^* = 1.74 \times 10^{-5}$  the supercooled liquid transforms sharply to an ordered solid at about  $T^* = 0.6$ , which analysis reveals is a quasicrystal (sometimes icosahedral and sometimes decagonal). The solid may still contain defects, but the order can be improved by annealing. The annealed structures are quenched down to  $T^* = 0$  for structure analysis. Subsequent annealing runs with  $5 \times 10^5$  steps at constant temperatures of  $T^* = 0.5$  and  $0.4$  show that the nucleated structures are stable in the sense that they do not change except for defect annealing. More details about the cooling simulations can be found by Roth et al. (1995).

The new decagonal structure was observed at cooling rates of  $T^*/t^* = 1.74 \times 10^{-6}$  and  $1.74 \times 10^{-5}$ . The tenfold axis is aligned with the  $\langle 110 \rangle$  diagonal of the cubic simulation cell; the structure is stacked periodically, with a stacking vector parallel to this direction. Fig. 1 shows a projection of the simulation box onto a plane normal to this axis; the atom positions are highly ordered and the approximant tenfold symmetry within this plane is obvious. Because of the constraint of fitting into the fixed, periodic simulation cell, the structure is distorted somewhat (in that the  $x/y$  ratio within the layers is squeezed relative to decagonal symmetry).

By examining slices transverse to the decagonal axis (not shown), we could distinguish three different types of layers transverse to the tenfold axis, which we label ‘‘A’’, ‘‘B’’, and ‘‘X’’. Let  $c$  be the lattice constant in the stacking direction; the simulation box extends over two periods ( $2c$ ) before encountering the same atomic layer. Most of the atoms in our structure are in A and B layers, which are separated by  $\sim 0.8$  units. The A layer (at height 0) consists mostly of pentagons linked by corners; the B layer (at  $c/2$ ) also consists of pentagons, but these are bigger and share edges instead. The basic motifs in the A/B layers are therefore pentagonal antiprisms. Both the A and B layers contain a mix of L and S atoms. Between the A and B layers at  $c/4$  and  $3c/4$  are the much sparser X and X' layers. These contain only S atoms centering the pentagons in the A/B layers, thus forming chains of interpenetrating icosahedra along the  $c$  direction. The X and X' layers are identical in projection on the quasiperiodic plane. The complete stacking sequence is AXBX'.

In order to discuss the structure in greater detail, it is convenient to present an idealized model; we shall do this in the next section.

The centers of the columns of icosahedra are shown linked by added lines in Fig. 1. Observe that the structures we found in simulations are not strictly periodic in the stacking direction: the axis centering a column of icosahedra may jump in position from one layer to the next.

We also observed icosahedral structures under the same simulation conditions. Consequently, both phases might coexist in single (larger) sample. Such a coexistence is well-known experimentally in the Al-transition metal structure family, most commonly among metastable, rapidly-quenched quasicrystals but also for stable phase i(AlPdMn) and d(AlPdMn) (Beeli, Nissen and Robadey, 1991). The simultaneous stability (or near stability) of both structures suggests that the local order is very similar. Indeed, we shall show that our decagonal structure model is quite closely related to the well-known ‘Henley-Elser’ (Henley and Elser, 1986) model.

### 3 Decoration Models

The most convenient framework for making sense of our structures, without any bias about the kind of long-range order, is a decoration of a tiling with atoms. The same decoration scheme, with a finite number of site types and positional parameters, can model a random structure as a decoration of a random tiling, or an ideal quasiperiodic structure as a decoration of a quasiperiodic tiling.

However, in attempting to describe an idealized structure model, we suffer from an embarrassment of riches. That is, there are several related structure models describing this kind of order. The models differ by (i) breaking a local symmetry in the position of an atom (which introduces matching-rule-like arrows) (ii) by allowing additional kinds of tiles (iii) by constraining the packing of tiles (this may create larger tiles as composites of smaller ones).

Structure models are conveniently presented using idealized positions, represented as integer

combinations of some finite set of basis vectors, but obviously the real atoms undergo displacements from these positions. Two structural models are called “topologically equivalent” (Mihalcovič et al. 1996a) when they converge to the same structure after equilibration at low temperature (or at zero temperature by relaxation under the pair potentials. Although apparently different, the models are physically indistinguishable. Thus the concept of topological equivalence is crucial in comparing different structure models and in organizing the above-mentioned family of related structure models.

We will begin (Sec. 3.1) with a simple simple tiling of three tiles – the fat and skinny Penrose rhombus plus distorted hexagon “Q” – from which the other tilings can be derived. This is not itself a good tiling model, because the packing is poor in the skinny rhombus, but it functions as a “zero-order” approximation for constructing better models. Therefore, we go on to consider two different modifications which correct this: (i) the triangle-rectangle tiling (Sec. 3.2). and (ii) the “two-level tiling” (Sec. 3.3) The relation of each modified model to the Penrose tiling decoration is an example of a “differentiation” in the terminology of Mihalcovič et al. (1996b); this means that a single environment in one model corresponds to several subclasses in the second model, which have somewhat different atomic decorations.

### 3.1 Basic Tiles

Next we present the simplest possible version of the model, phrased as a decoration of the Penrose rhombi without matching rules.

#### 3.1.1 Penrose Rhombi

Consider the decoration of the fat and skinny Penrose rhombi, as shown in Fig. 4(a,b). This structure is not the best packed, but it is certainly one of the simplest. Each large atom is at a position dividing the long diagonal of a fat rhombus in the ratio  $\tau^{-1} : \tau^{-2}$  where  $\tau$  is the golden mean  $(1 + \sqrt{5})/2$ . Notice that there is a complete symmetry between the A and B layers. Furthermore, the decorating atoms sit on the midpoint of each tile edge, so the decoration does not enforce the Penrose matching rules: it may be applied to any random tiling of these rhombi.

The centering atoms of the pentagons are called  $\alpha$ . They are located in the X layer at the corners of the rhombi. In the A layer, the mid-edge atoms are called  $\beta$  and the rhombus interior atoms  $\lambda$ . In the B layer, the equivalent mid-edge atoms are called  $\gamma$  and the rhombus interior atoms are  $\mu$ .

There are two alternative criteria for assigning the species: either according to interatomic distances in the model, or according to coordination number (Henley and Elser, 1986); the two criteria are obviously correlated and (for all models presented in this paper) they lead to the same assignments. We assign  $\beta/\gamma$  mid-edge sites to be S atom, since they have coordination 12 and tend to be squeezed by the  $\alpha$  atoms at either end of the edge. The  $\alpha$  sites are also assigned S atoms, since they have coordination 12 and are squeezed along the  $z$  axis where they form chains. (The interlayer spacing is less than an interatomic spacing, since the other atoms don’t form vertical chains.) Finally, the  $\lambda/\mu$  sites, which all gave coordination 16, are taken to be L atoms.

#### 3.1.2 Q Tile

In the Penrose decoration, described so far, the A and B layers are equivalent by a  $10_5$  screw symmetry, and correspondingly  $\beta$  is equivalent to  $\gamma$  and  $\lambda$  is equivalent to  $\mu$ . However, in the decorations we present later, the A and B layers will be inequivalent. In those more complicated structures, a single Greek label refers to several subclasses of atoms having similar but not identical local environments. (Usually their coordination shells are topologically identical, but there is some variation in which neighbors are L and S atoms.)

The Penrose tiling structure forces a “short” linkage between two vertices when they are related by the short diagonal of the skinny rhombus. Here “linkage” denotes a connection between the centers of neighboring motifs, which form the vertices of a rigid network. (In this case, the motif is

the chain of centered pentagons, and the network is the tiling.) The  $\alpha$  atoms projecting to those two vertices have *non*-icosahedral coordination shells. (There are similar to the awkward coordination shells occurring in the oblate rhombohedron (Henley and Elser, 1986)). We believe these are unfavorable energetically. (Indeed, nothing resembling a skinny rhombus is found in Fig. 1.) Therefore, we shall make an additional hypothesis: *true chains of icosahedra are energetically favorable and so their frequency should be maximized.*

To increase the number of chains of icosahedra, we must somehow eliminate the short linkages. This is possible whenever two skinny tiles and a fat tile form a distorted hexagon; they can be joined in a composite tile Q as shown in Fig. 4(c). The only change in atomic positions in forming the Q tile is along the axis over the central vertex, where the the  $\alpha$  atoms forming the chain are replaced by  $\lambda'$  atoms (in A layers, if the adjacent atoms along the tile edges are in a B layer, and otherwise vice versa). Note there are half as many new atoms  $\lambda'$  as there were of old  $\alpha$  atoms; they should be L atoms because of this larger spacing (or alternatively, because they have coordination 15). We will call this operation a “chain-shift”.

Note that the Q tile is considered to have a symmetry between the top apex and bottom apex (the light dashed lines in Fig. 4(c) only illustrate the topological equivalence to the apparently asymmetric Penrose tile decoration.) The Q decoration should have the full symmetry of the Q tile’s exterior; after the chain-shift, this require only small adjustments of position and species. The  $\lambda$  site from the fat tile is renamed  $\lambda'$  since it has coordination 15 after the chain-shift and is symmetry-equivalent to the  $\lambda'$  site from the internal vertex. The non-Frank-Kasper  $\gamma$  atom on the edge shared by skinny rhombi is converted into a  $\mu$  L atom (upper part of Fig. 4(c)) just like the  $\mu$  site from the fat rhombus.

Finally, the other two non-Frank-Kasper  $\gamma$  sites on internal edges are renamed “ $\delta$ ” and must be shifted slightly so as to lie symmetrically on the bisector of the long Q diagonal (since their neighbors are symmetric around that bisector.) They divide the bisector line almost into thirds (we used 0.312 : 0.376 : 0.312 in the initial configuration for simulations in Sec. 5.1). Since the  $\delta$  atoms have coordination 14, and are somewhat squeezed with their neighbors along the bisector line, they have been designated S atoms. (However, note that coordination 14 was found to be borderline in the closely related icosahedral structure: analogous sites occurring on the short axis of the rhombic dodecahedron tile (see below) are occupied by small atoms in  $i(\text{AlCuLi})$  but by large atoms in  $i(\text{AlMgZn})$ (Henley and Elser, 1986)).

To maximize the number of proper centered-pentagon chains, then, the original tiling should be arranged with skinny rhombi grouped in pairs wherever possible. This is essentially the same mathematical problem as that of packing equal disks on Penrose tile vertices (Henley, 1986); those the disks correspond to the pentagon-chain motif in the present model.

### 3.1.3 Icosahedral Tiling Relationship

It is interesting to note the close relationship of this tiling to the three-dimensional “Henley-Elser” decoration of the Ammann rhombohedra by L and S atoms as a model of Frank-Kasper icosahedral quasicrystals such as  $i(\text{AlCuLi})$  and  $i(\text{AlZnMg})$ . Let us orient rhombohedra so that one edge lies in the vertical direction as shown in Fig. 2, but shear them slightly so that the vertical edge has length  $c$  and the other five kinds of edge have vertical component  $c/2$  and horizontal components of length  $a$  along one of the five basis vectors.

Projecting the prolate and oblate rhombohedra onto the plane perpendicular to the selected axis generates respectively the fat and skinny rhombus of the (2D) Penrose tiling. Thus, every tiling of the rhombi can be extended vertically as a stacking of rhombohedra with period one edge length along the special axis. The layer of this stacking is a puckered slab dual to a grid-plane, analogous to one of the “tracks” in a two-dimensional Penrose tiling (Katz and Duneau, 1986). Note that, in contrast to a generic rhombohedral tiling, *every* rhombohedron in this stacking has edges in the vertical direction.

In fact, it turns out that our decagonal decoration of Penrose tiles is “topologically equivalent” to the icosahedral decoration of rhombohedra by Henley and Elser (1986) <sup>1</sup>.

<sup>1</sup>A similar, but quite imperfect, relationship can be made between the icosahedral  $i(\text{AlMn})$  (Elser and Henley

To see this, cut the rhombohedra along horizontal planes such as those shown dashed in Fig. 2(a,b) – all the atoms in the PR and OR lie in or near these rather densely packed layers. Then reassemble them into prisms with horizontal rhombic faces. The atom positions form a decoration of the prisms, shown in Fig. 2(c,d), which is clearly equivalent to that in Fig. 4(a,b). (The ideal positions by Henley and Elser (1986), projected onto the plane, are *exactly* those used here in the tiling; the vertical positions of the  $\lambda$  atoms, however, must be adjusted by  $\sim 0.026c$ .)

The third tile of the Henley-Elser model, the rhombic dodecahedron (RD), is a little bit more complicated. (see Fig. 3). Before it can be stacked, two skew triangular prisms at opposite sides of the RD, forming together one PR, must be removed. If this truncated RD is cut into layers and reassembled, it produces an elongated hexagonal prism which is decorated exactly as the Q tile in Fig. 4(c).

The structure obtained by transforming the Henley-Elser structure not only has the atoms in exactly the same positions (after the small vertical shifts) as our decagonal model, but also has exactly the same assignment of S and L atoms. That is not very surprising, since the species were assigned according to the local environments in both models.

### 3.2 Triangle-Rectangle Tiling

Returning to the 2D tiling, there are now two possible schemes to handling the skinny rhombi everywhere in the tiling. In one scheme, we imagine first that *all* skinny tiles are paired and absorbed into Q tiles: a generic tiling of this sort is the “fR/Q (fat rhombus and Q) tiling”.

Then the Q tile can be divided into a rectangle (R) and two isosceles triangles (T), with new edges of length  $b \equiv (1 + \tau^{-2})^{1/2}a$ , while each rhombus can be divided into two isosceles triangles of the same kind. The two objects can form random tilings of the plane, most of which cannot be regrouped into rhombi (Oxborrow and Mihalkovič, 1995). The decoration introduced in this paper is compatible with an arbitrary triangle-rectangle (T/R) tiling. Note that, in this variant of the structure model, each tile comes in an A and a B flavor, denoting the level at which its mid-edge atoms sit; tiles adjoining each other by a  $b$  edge have opposite flavors.

The triangle and rectangle have long been known as the building blocks for the so-called pentagonal Frank-Kasper phases (see for example Samson (1968); Samson (1969)). The 12-fold symmetric quasicrystals, which are typical Frank-Kasper phases, are built from a triangle and square on which the atomic arrangements are similar, but not identical, to those in the T and R tiles in our model. Furthermore, a T/R description like ours was used by He et al. (1990) to describe the  $\text{Fe}_{52}\text{Nb}_{48}$  quasicrystal, the only real material claimed to be a Frank-Kasper decagonal. (See Sec. 6.4; Nissen and Beeli (1993) also used a rhombus-triangle-rectangle tiling to analyze TEM images of a Fe-Nb decagonal quasicrystal.) However, the decagonal T/R structure has been systematically studied as an abstract (random) tiling only recently (Oxborrow and Mihalkovič, 1995; Cockayne, 1994).

We shall now consider energy differences between different T/R tilings which might cause additional ordering. It would seem unfavorable energetically for two rectangles to adjoin along an  $a$  edge, since the  $\delta$  and  $\beta/\gamma$  atoms along the bisecting axis are tight within each tile and would be squeezed against each other; let us add this to the constraints defining our tiling ensemble. Then Cockayne’s quasiperiodic T/R packing (Cockayne, 1994) satisfies the constraint just mentioned; it satisfied a second constraint, in that rectangles don’t adjoin along  $b$  edges, either. With the latter constraint, every rectangle must be capped with triangles forming a complete Q tile, and then all other triangles must be paired along their  $b$  edges forming complete fat rhombi: thus the structure is more economically described as an fR/Q tiling with the constraint that Q’s may not lie side-to-side. (We presume the ensemble of such packings is a random tiling, but this is not proven.) Every fR/Q structure, of course, can be considered as a fat and skinny (fR/sR) rhombus tiling produced by decomposing the Q tile. It has been pointed out (Mihalkovič, 1995; Oxborrow and Mihalkovič, 1995) that an fR/Q tiling gives the optimal disk packing (i.e. maximal density of  $\alpha$ -chains, in our models) of all Penrose tiling, since *all* the skinny rhombi are grouped

---

1985; Mihalkovič 1996b) and the decagonal model based on the  $\text{Al}_{13}\text{Fe}_4$  structure (Henley, 1993)

into pairs, unlike the two-level tiling described below.

Possibly the additional constraint on the T/R tiling is justified by the energetic cost of adjoining along the  $b$  edge – the  $\lambda'$  atoms inside one R press against the  $\delta$  atoms (in the same layer) inside the other R – but we have not identified any compelling argument and hence do not propose the fR/Q tiling as the optimal geometry.

### 3.3 Two-Level Tiling

The decagonal structure observed after cooling from the melt (Sec. I) had the additional property that its A layer is inequivalent to its B layer. We shall now turn to a structure model which adopts this as a postulate. Chain-shifts occur only at vertices where all the edges are decorated with B layer atoms. Naturally, the B atoms in turn shift away from the midpoint of the edge towards the partially vacated columns. (This was observed in the simulation, in the fact that the B layer pentagons were bigger than A layer pentagons.) This has the effect of the double-arrow matching rule in the Penrose tiling. An arbitrary tiling obeying only the double-arrow matching rules (Tang and Jarić, 1990) is equivalent to a random tiling of three composite supertiles Q, K, and S<sup>2</sup> which are obtained by merging Penrose tiles along the double-arrow edges. Since the atoms decorating the outer edges of the Q, K, and S tiles remain symmetric about the middle of the edge, they do *not* enforce the (single-arrow) Penrose matching rules on these edges: all random tilings of the plane by Q, K, S tiles are a priori permissible. The random tiling of these tiles has been called the “two-level” tiling (2LT)(Henley, 1991a); these tiles were independently proposed by Li and Kuo (1991). Fig. 5 shows a fragment of the 2LT, including one of each tile. As a special case, the Penrose tiling, modified by combining rhombi along their double-arrow edges, becomes a simple quasiperiodic Q, K, S tiling.

The “Q” tile decoration was described already; the star tile S is also straightforward, being a composite of five fat rhombi. Note that no chain-shift is necessary at the center of the S tile since there is no skinny tile adjoining; thus this site forms an exception, around which the A/B symmetry breaking (between large and small pentagons) is opposite to the pattern around all other  $\alpha$ -chains. Otherwise, all the edge sharing pentagons are in layer A and the corner sharing pentagons are in layer B.

The “K” tile is a grouping of a skinny rhombus with three fat rhombi; there is a chain-shift on the central vertex, which becomes known as a  $\kappa$  site. This is the second option for absorbing the extra single skinny rhombi, instead of pairing all of them in Q tiles. However, the atomic arrangements in the K are still somewhat awkward. The four  $\gamma$  atoms surrounding the internal vertex can only relax to form a sort of pentagon with a missing corner, meaning that the  $\kappa$  coordination shell is not a Frank-Kasper polyhedron but a distorted octahedron.

We could have arrived directly at the two-level tiling from analysis of Fig. 1, if we accepted as a postulate that in the linkage between two chain-motifs, the edge-sharing pentagons are always in the B layer. We quickly arrive at a geometry where the angles between linkages are all multiples of  $2\pi/5$ . The smallest tiles enclosed by such edges are the Q, K and S tiles of the “two-level” tiling (Fig. 5). The details of this derivation are in Appendix A.

Reviewing Sec. 3, we can identify a hierarchy of successively more ordered tiling geometries. The Penrose tiling is the most ordered; it can be broken up into the “two-level” tiling of Q, K, S tiles. The K and S tiles can be broken up further into fat and skinny rhombi; finally the fat rhombi can be broken into triangles, and the Q tiles broken into triangles and rectangles.

## 4 Quasiperiodic Models and Stoichiometry

Even when a quasicrystal model has been formulated as a tile decoration, it is often illuminating to represent it as a quasiperiodic structure obtained by a cut through a higher-dimensional space, since (i) the space-group and diffraction properties are most concretely understood in this fashion

<sup>2</sup> The three tiles are called “Q, K, S” after the corresponding three local environments found in the Penrose tiling where double-arrow edges can meet. The same tiles are called “h,c,s” respectively by Li and Kuo (1991).

(ii) different site types are represented as domains of the acceptance domains in the “perp” space, thus the relations between different site types are visible in the spatial relation of the domains. (iii) The number density (or frequency) of a particular species or site type is proportional to the area of its portion of the acceptance domain, which is convenient for computing a definite stoichiometry.

This description is helpful even for atomic models based on random tilings. These, when ensemble-averaged, produce structures of partially-occupied sites. Mapped into perp space, such distributions can usually be *approximated* as quasiperiodic acceptance domains convolved with a Gaussian in perp space (Henley, 1991a).

The first step is to find a quasiperiodic tiling. This is trivial for the two-level (Q/K/S) tiling, but highly nontrivial for the T/R (or for the fR/Q) tiling; in that case, the tiling can only be constructed by an elaborate deflation, and the corresponding acceptance domains have fractal boundaries (Cockayne, 1994). Therefore, we will limit ourselves to presenting the acceptance domains based on the Q/K/S-tiling decoration, where the tiles are arranged in the perfect Penrose tiling. (A Penrose tiling is turned into a two-level (Q/K/S) tiling simply by erasing the double-arrow edges).

Also in this section, we tabulate the contents in atoms of each tile. This approach to stoichiometry is a more powerful than the approach using the acceptance domain, since it can be applied even to random tilings.

#### 4.0.1 Idealized Structure and Acceptance Domain

In order to construct the acceptance domain, we first make a crude idealization of the Penrose-rhombus decoration which we presented first (Fig. 4(a,b)). All  $\beta$  atoms lie on single-arrow edges and all  $\gamma$  atoms lie on double-arrow edges. Let us shift the  $\beta$  atoms and the  $\gamma$  atoms in the direction of Penrose’s arrows, such that each divides its edge in the ratio  $\tau^{-1} : \tau^{-2}$ . (This ratio is technically convenient in allowing the ideal coordinates to be written as integer combinations of the five basis vectors. They are actually most simply treated using a deflated Penrose tiling basis with lattice constant  $\tau^{-1}a$ .)

In going to the Q/K/S tiles for in the quasiperiodic structure, we retain these same positions but change the label and the species as described in Sec. 3.3; note in particular that the displacement properly places the  $\delta$  atoms on the bisecting symmetry axis of the Q tile. The B layer forms Penrose’s packing of regular pentagons, one centered on every vertex of the 2LT. Each “internal” vertex (where double-arrows meet) is also surrounded by a pentagon, but these are irregular and have many short distances.

The acceptance domains are shown in Fig. 7. Note there is a separate domain for layers A, B, and X of the real structure; in addition, as always, the vertices project into five flat two-dimensional layers in three-dimensional perp-space, so we must show separate shapes for each perp-space layer. Finally we have shaded the domain with dark and light shading to distinguish L and S atom occupancy.

Although this structure has unreasonable distances, it is “topologically equivalent” (Mihalcovič et al. 1996a) to the (reasonable) version presented in figure 5. We could alternatively compute the acceptance domains for the decoration in figure 5, with the atoms moved to mid-edge positions (except for those in the Q tile). Relative to Fig. 7, the  $\beta$ ,  $\gamma$ , and  $\delta$  subdomains each would get broken up into five pieces, and shifted in the parallel space direction. Since the mid-edge atom positions are also special crystallographic positions, several of the shifted subdomains will reunite there and form a new piece of acceptance domain which is centered on a mid-edge site in the 5-dimensional hypercubic lattice. We forgo to present these domains since this second picture is less compact and not as appealing as the first one.

The space group of this quasiperiodic decoration is  $P10/mmm$ . In other variant decorations in which the A/B symmetry is not broken, we would get an additional system of mirror planes perpendicular to the 10-fold axis and this changes the space group to  $P10_5/mmc$ . The point group of the motif with the highest symmetry is  $5/m\bar{m}$  (Henley, 1993).

### 4.0.2 Stoichiometry

The most general approach to stoichiometry is to count the number of atoms associated with each tile. Table I summarizes the contents of each tile. The combination Q+S has contents 29L+14S while 2K (which covers the same area as Q+S) has contents 28L+14S. This suggests that the K tile is too loosely packed; indeed, the average coordination number in K is also a bit low.

Table II gives the coordination numbers and the net stoichiometry for each decoration. In the case of the 2LT (Q/K/S) decoration, this agrees with the stoichiometry which can be read off from Fig. 7. It can be seen that the stoichiometry is close to  $LS_2$  in both cases. (The pure Penrose tiling decoration, an unrealistic model, has  $L_{0.198}S_{0.802}$ .) That seems to be considerably fewer L atoms than in the T(AlZnMg) icosahedral approximant (Bergman, Waugh and Pauling, 1957) or Samson’s AlMg-type structures, but it is comparable to  $i(\text{Al}_6\text{CuMg}_3)$  in which only 30% of the atoms are L (Mg) (Samson, 1968; Samson, 1969).

## 5 Further Simulations

In section III, we worked out the geometric properties of the idealized model, in several closely related variants based on different tiling rules. We derived the coordination configuration for all sites: all atoms have a reasonable distance from their neighbours and most of them are tetrahedrally close packed.

The idealized model, in any of the variants presented in the last two sections, is well-packed and (nearly) tetrahedrally close-packed around every atom. Hence it is expected to be (locally) stable against disordering by thermal fluctuations. To check this stability, we ran additional simulations starting with a configuration from the ideal model.

A major motivation of these simulations was to locate the region of parameter space in which the quasicrystal phase may be thermodynamically stable; hence, we attempted to adapt the potentials to the structure model, as explained in Subsec. 5.1. As a result of the optimization there we can predict the ideal  $c/a$  ratio and the density of the structure, as well as the ratios of bond radii for LL, LS and SS pairs which seem most conducive for (decagonal) quasicrystal-forming.

We used not only Lennard-Jones (LJ) potentials as in eq. (1) but also the Dzugutov potential, with independent parameters for the three ways of pairing species  $\alpha$  and  $\beta$ . Both pair potentials have a single attractive well with a minimum at radius  $2^{1/6}\sigma_{\alpha\beta}$ , and having depth  $\epsilon_{\alpha\beta}$ ; here  $\sigma_{\alpha\beta}$  and  $\epsilon_{\alpha\beta}$  are called the “bond parameter” and “interaction parameter”. The Dzugutov potential (Dzugutov, 1993) has an additional repulsive maximum at a radius  $\sim 1.6$  times that of the minimum, and a height  $\sim 0.5\epsilon_{\alpha\beta}$ ; this is designed to disfavor the square arrangements found in fcc, bcc or hcp structures.

### 5.1 Optimization of Parameters

To find the optimal potential parameters, we minimized the potential energy at  $T = 0$  while varying these parameters. For this purpose we used a fixed ideal structure model with the ideal atom position and without relaxation. The sample size was a  $p/q = 3/2$  approximant<sup>3</sup> of a perfect Penrose tiling with 10 periods of XAXB layers and ideal size  $l_x \cdot l_y \cdot l_z = 18.95 \cdot 16.09 \cdot 22.93$ , containing 3270 small and 1420 large atoms. Samples of different size do not yield different results within the accuracy we achieve.

In a three-dimensional structure with two species of atoms L and S, bond and interaction parameters  $\sigma_{\alpha\beta}$  and  $\epsilon_{\alpha\beta}$  must each be determined for pairs  $\alpha\beta$  equal to  $LL$ ,  $LS$ , and  $SS$ . Of course, one of the  $\epsilon_{\alpha\beta}$ ’s can be eliminated in principle, in the choice of the energy unit. We chose the sample size/shape (which was kept fixed in the  $xy$  plane of the layers) so as to the Penrose tile edge length at exactly  $a = 2$  (the nearest-neighbour distance is roughly  $a/2$ .) Thus all three  $\sigma_{\alpha\beta}$ ’s are nontrivial parameters.

<sup>3</sup> the basis vectors are  $(2q, 0)$ ,  $(p - q, p)$ ,  $(-p, q)$ ,  $(-p, -q)$ ,  $(p - q, -p)$ , and the periods are  $2(2p - q)\tau + 2(3q - p)$  in  $x$ -direction and  $4\sin(\pi/10)(p\tau + q)$  in  $y$ -direction.

Results obtained in optimizing potentials for binary icosahedral Frank-Kasper structures (Roth et al. 1990) with similar local structure and potentials, show that  $\sigma_{\alpha\beta}$  are largely independent of  $\epsilon_{\alpha\beta}$ , for  $\epsilon_{\alpha\beta}$  in the range of  $0.5 < \epsilon_{\alpha\beta} < 2.0$ . Therefore we set  $\epsilon_{LS} \equiv 1$  and  $\epsilon_{LL} = \epsilon_{LS} \equiv 1/2$ . Thus, we actually varied only the three  $\sigma_{\alpha\beta}$ 's.

Before we can carry out the optimization itself we have to determine the lattice constant  $c$  in the stacking direction. (The A/B layer spacing  $c/2$  should also be roughly a lattice constant.) This is done in a poor man's minimization by scanning the interval  $0.8 < c < 4.0$  and looking for the minimum of the potential energy  $E(c)$  in the following way: having fixed  $a$  (and consequently  $l_x, l_y$ ) we calculate the partial radial distribution functions  $g_{\alpha\beta}(r)$  for the ideal model using a given layer distance  $c$ . Then, without annealing or relaxing, we compute the partial potential energy

$$E_{\alpha\beta}(\sigma_{\alpha\beta}, c) = \int_0^{r_c} v_{\alpha\beta} \left( \frac{r}{\sigma_{\alpha\beta}} \right) g_{\alpha\beta}(r, c) 4\pi r^2 dr \quad (2)$$

dependent on the cut-off radius  $r_c$  and the pair potential  $v_{\alpha\beta}$  and minimize it as a function of  $\sigma_{\alpha\beta}$ . Using this procedure we find that the total potential energy  $E = E_{LL} + E_{LS} + E_{SS}$  is minimized if each  $E_{\alpha\beta}$  is optimized separately.

The optimal  $\sigma_{\alpha\beta}$  for Lennard-Jones potentials are  $\sigma_{SS} = 1.029$ ,  $\sigma_{SL} = 1.137$ , and  $\sigma_{LL} = 1.189$ . For the potentials used by Dzugutov we get  $\sigma_{SS} = 1.108$ ,  $\sigma_{SL} = 1.034$ , and  $\sigma_{LL} = 0.929$ . The result reflects the fact that the Dzugutov potentials are very short ranged and that they have a maximum repulsive for second nearest neighbours, whereas even in the cut-off and smoothed version of the Lennard-Jones potential interactions with the second or third set of neighbours are still attractive.

We also found that the optimal A/B interlayer distance for Lennard-Jones and for Dzugutov potentials is about  $c/2 = 1.04 \pm 0.01$ . The uncertainty quoted here reflects the slight variation of the spacing depending on the choice of  $\epsilon_{\alpha\beta}$  and  $r_c$ .

## 5.2 Results

The constant temperature and pressure molecular dynamics simulation method described in Sec. 2 has been applied to study the thermodynamic stability of the ideal structure. To simulate non-cubic structures it has been extended to allow independent changes of the box lengths  $l_k$ . Thus during the MD simulations the box size could vary in contrast to the optimization, where the box was fixed. The simulation sample was the same as the one used in Sec. 5.1. With Dzugutov's potentials the melting temperature at  $P^* = 0.01$  is  $T_m^* = 1.23$ . (In fact, the structure does not melt; it vaporizes.)

Of course, in an infinite box the ratio  $l_x/l_y = 2 \sin 36^\circ \sim 1.1756$  is fixed by pentagonal symmetry. In a finite system, however,  $l_x/l_y$  should deviate slightly from the ideal ratio due to the "phonon-phason" coupling (Lubensky, 1988, and references therein) since the periodic boundary conditions force a nonzero phason strain. We found the equilibrium value  $l_y/l_x = 1.177$  in the simulation, independent of the temperature and very close to the ideal value.

The A and B layers are mirror planes so they should still be flat in the relaxed structure; on the other hand, the X layers should pucker slightly after relaxation, with the X' layer puckered in the opposite direction. The simulation, however, show that the layers remain essentially flat.

We have also recorded the atomic mobility by monitoring the mean square displacement of the atoms. It turns out that even close to the melting point ( $T = 0.9T_m^*$ ) long-range diffusion is *not* observable at all, and only very few atoms are seen to jump to a new position. Those atoms which do jump are all in the skinny rhombus part of the K-tile. Similar results have been obtained for icosahedral and dodecagonal structures (Gähler and Roth, 1995) where oblate rhombohedra and skinny rhombic prisms resp. play the same role as the flat rhombus in the K-tile.

Most of the jumps in the K tile take place around the  $\alpha$  atom at the top of the tile (see Fig. 5) and around the interior vertex. Possibly the jumping in this environment indicates that our model is erroneous there: perhaps a different arrangement or choice species should occur in the atoms surrounding the interior vertex of the K tile, or perhaps the correct model is a T/R tiling which

has no K tiles at all. It is also possible that the correct structure model should be thought of simply as a random tiling of Penrose rhombi (Sec. 3.1.1); then “phason fluctuations” are realized by tile flips that entail switching which vertex of a skinny rhombus undergoes a “chain-shift”.

Our conclusion is that the structure is very stable, and that the choice of the atoms positions is reasonable. The jumping atoms do not affect the stability since they are separated by large distances.

## 6 Discussion

### 6.1 Summary

Now we are back at the beginning: we started with a structure found by computer simulations, and recognized that the structure could be described by a tiling model. We derived quite a number of tilings involving fR, sR, T, R, Q, K, and S tiles, all of which are compatible with a decoration with atoms that include the original model. Although the fR/Q and T/R models seem to be superior to the Q/K/S tiling and the variants involving sR tiles, there may be properties that favour the latter. We tested one variant (Q/K/S) of the tiling models again with computer simulation to derive structure and potential parameters, and to find out if the geometrically reasonable model is also reasonable with a simple interaction model. Since the Q/K/S tiling is somehow cumbersome, but on the other hand includes most of the properties of the other tilings, its stability assures us that the other tiling types will also be stable.

Up to now we have only treated each tiling for itself and described its properties. In this final section we would like to address the interrelationship of the tiling types, and if there is a hierarchy of tilings. This includes the A/B layer symmetry breaking which occurs in some of the models. In addition to computer simulations it will be interesting to compare the tiling models to experiment and to other structure models. Furthermore we want to ask if and how it is possible to change a certain tiling which means reshuffling the tiles, introducing defects like random stacking and atomic jumps. These moves may also lead to the a transformation of one tiling type into another. Although such a process is not suitable for MD simulations, it may be studied in Monte Carlo simulations with properly chosen interactions.

### 6.2 Hierarchy of Tiling Descriptions

Our approach is an example of a general approach which may be fruitful in understanding the relation of interatomic interactions to long-range order in quasicrystals. An ensemble of tilings is proposed; via a decoration rule, these correspond one-to-one to an ensemble of low-energy atomic structures. However, the energy is slightly different for each of these structures; these energy differences may be considered as a “tiling Hamiltonian”  $\mathcal{H}_{tile}$  which is purely a function of the tile arrangement. Often the tiling Hamiltonian is a sum of one-tile and neighbor-tile pair interactions (Mihalcovič et al. 1996a,1996b) ; alternatively, Jeong and Steinhardt (1994) proposed a family of tiling Hamiltonians with a (favorable) energy  $-V$  for each occurrence of a special local pattern, which they called the “cluster”.

The ground states of  $\mathcal{H}_{tile}$  are a subset of the original ensemble; most often this constrained sub-ensemble can be described by a tiling of larger (“super”) tiles with their own packing rules. In the “cluster” Hamiltonians studied by Jeong and Steinhardt (1994), the degree of long-range order is enhanced in the supertiling – indeed for one special “cluster” one just obtains the quasiperiodic Penrose tiling – and even a random tiling of supertiles has greatly reduced phason fluctuations.

Evidently, if  $\mathcal{H}_{tile}$  can be divided into a sum of successively weaker parts, there may be a corresponding hierarchy of successively larger supertiles. Furthermore, as the temperature is raised, the constraints due to the weakest terms of  $\mathcal{H}_{tile}$  are broken, so the size of the relevant tiles may decrease with temperature. (The associated changes in diffraction pattern were discussed by Lançon, Billard, Burkov and de Boissieu (1994)). In Sec. 3 , we discovered just such a hierarchy of similar structures, some more constrained than others, as follows: the fR/Q tiling is a special case

of either the fR/sR/Q (fat and skinny rhombus and Q) tiling, or of the T/R tiling. The 2-level (Q/K/S) tiling is also a special case of the fR/sR/Q, which is a modification of the fR/sR tiling (Subsec. 3.1).

We postulated (at the start of Sec. 3) that the dominant term in our tiling-Hamiltonian favors the chain-motif, consisting of  $\alpha$  atoms surrounded by alternating pentagons. (Incidentally, this is a “cluster” in the sense of Jeong and Steinhardt (1994).) Then the sub-ensemble which minimizes that term is the T/R random tiling, which (see below) is also consistent with a structure model proposed by He et al. (1990).

Due to the limitations of our simulation, and because we did not perform relaxation at  $T = 0$  to extract the parameters of  $\mathcal{H}_{tile}$ , we could not prove that the chain-motif (and hence T/R tiling) is favored, nor could we measure the smaller energy differences that would decide which subensemble of T/R tilings most faithfully models the structure. We could only conjecture (in Sec. 3.2) that there should be an additional term in  $\mathcal{H}_{tile}$ , disfavoring Q tiles adjoining by  $a$  edges. Granting that, it followed that the best tiling to represent our structures is something between the T/R tiling and the fR/Q tiling of Cockayne (1994).

### 6.3 Issues of Symmetry Breaking in our Simulation

There remains a serious doubt that the apparent decagonal structure we observed in our simulations might be only an artifact of the geometric restrictions imposed by the small simulation box: the correct phase in the thermodynamic limit might be an icosahedral random tiling. Indeed, Sec. 3.1.3, showed that our decagonal structure is essentially a special layered packing of the icosahedral tiles; rhombohedral tiling might find a layered arrangement in a quench, if that happens to fit well with the periodic boundary conditions. Furthermore, out of seven quenches with the same potentials (Roth et al. 1995), five quenches led to icosahedral structures and two to decagonal ones.

Even if we grant that the true structure *is* decagonal, there is a second question whether we may be over-interpreting accidental effects of the finite-size box used in our initial simulations: does an A/B symmetry-breaking occur in the thermodynamic limit? This is the fundamental difference between the 2LT (Q/K/S) model and the T/R tiling model. Apart from the observation in our initial simulation, there is no convincing reason for the 2LT (Q/K/S) model, since the K tile seems to be poorly packed. There is no other numerical evidence that the A/B symmetry-breaking really occurs in an extended structure. It is quite possible that the shape and size of each layer in our simulation box happened to allow only a tiling which lacks the  $180^\circ$  symmetry axis (out of the plane) which would make A and B edges equivalent.<sup>4</sup>

To pursue this further, we should consider whether there is any physical cause for such a symmetry breaking. Rather than start with the Q/K/S tiles, it may be better to start by imagining a fR/sR/Q tiling and asking what might drive the symmetry breaking, which from this viewpoint is a displacive instability of the  $\gamma$  atoms, perhaps coupled to some chain-shifts. (After all, on every skinny rhombus such a symmetry-breaking occurs locally; the question is whether the pattern of displacements can be propagated from one skinny to the next.) It is plausible that, once A/B symmetry breaking is granted, it will be advantageous to group the rhombi into S and K tiles.

Both of these questions might be addressed (at zero temperature) by relaxing a variety of decagonal and icosahedral structures under a variety of potentials, to see which is more stable energetically, in the spirit of calculations done on some Al-transition metal quasicrystals (Phillips and Widom, 1994; Mihalcovič et al. 1996b) .

---

<sup>4</sup> A simple matching rule has been given that favours the Q/K/S tiling over T/R and fR/Q: if you consider the pentagonal antiprisms around the  $\alpha$  atoms, then there should always be two different atoms on the opposite sides of a diameter (true in the Q/K/S case). In the T/R tiling there are only two vertex environments that fulfill this condition, in the fR/Q tiling, there is only one. But with this vertex environments alone it is not possible to produce a fR/Q or T/R tiling. Thus the Q/K/S tiling is favoured. The rule also works if you have sR tiles: In an sR/fR and an sR/fR/Q tiling it either forces the assembly of Q/K/S tiles or induces chain shifts.

## 6.4 Comparison to Other Structure Models

The Fe-Nb structure model outlined by He et al. (1990) was not formulated in terms of a tiling of any kind, nor as a deterministic rule for packing the plane with motifs; instead, it is largely a scheme for analyzing high-resolution images. Although there is a possibility that they misinterpreted images of a periodic approximant of the quasicrystal, or a microcrystalline mixture of approximants, it is still interesting and economical to describe it using quasicrystal tiling element.

Their model is based on the same motifs (pentagon-chains) as ours and the lines in figure 3(b) of He et al. (1990), which indeed outline triangle and rectangle tiles, are the same as the  $a$  linkages in our model. Since the sample they imaged was rather small and defective (much like our first simulation), we can only be tentative which variant of our structure model it should be identified with. In principle a T/R tiling could be a  $\mathbb{R}/\mathbb{Q}$  tiling with the  $b$  edges drawn in. However, the image of He et al. (1990) includes pairs of rectangles adjoining by a  $b$  edge, which is a defect from the  $\mathbb{R}/\mathbb{Q}$  viewpoint; note also it clearly does *not* have a A/B layer ordering. Thus it is most plausibly idealized as a random T/R tiling;

The icosahedral relationship described in Sec. 3.1.3 allows the decagonal structure to grow on the icosahedral one. Congruent icosahedral/decagonal grain boundaries should therefore be possible. The decagonal phase could be viewed as an approximant to the icosahedral phase, and thin decagonal bands in the icosahedral phase may be regarded as stacking defects. Furthermore, since the icosahedral and the decagonal phases are similar in composition, phase transformations between them should also be possible. Thus our Lennard-Jones system might serve as a toy system for investigating the behavior *i*-AlPdMn. (However, we must re-emphasize that the atomic arrangement in an Al-transition metal quasicrystal certainly differs from the Frank-Kasper quasicrystal described here.)

We turn briefly to another approach to constructing structure models – that based on atomic clusters (Elser and Henley, 1985; Henley and Elser, 1986; Mihalcovič et al. 1996a), not to be confused with the “clusters” of Jeong and Steinhardt (1994)! Now, Al-Mn type structure models have a common motif of  $\text{Al}_6\text{Mn}_4$  tetrahedra (Kreiner and Franzen, 1995); by joining several of these along their faces larger clusters are formed which are also observed in these structures. On the other hand, Frank-Kasper models have a common motif of “truncated tetrahedra” surrounding every L atom with coordination 16; indeed, this motif is frequent in our structures. (see Fig. 8; the full coordination shell, with 4 additional atoms, is the “Friauf polyhedron”.) These are combined into larger clusters (Samson, 1968; Samson, 1969) in exactly the same fashion. Thus, if an Al-Mn model can be represented as packing of  $\text{Al}_6\text{Mn}_4$  tetrahedra (plus atoms needed to fill the interstices), then by replacing each of these by a truncated tetrahedron we produce a (hypothetical) Frank-Kasper model. For example, the “Mackay Icosahedron” (Elser and Henley, 1985) is a combination of 20 tetrahedra which maps to the Bergman polyhedron (Bergman et al. 1957). It is well known that that crystal phases  $\alpha$ -AlMnSi and *R*-AlCuLi are bcc packings of the respective clusters, and this suggested that the same cluster-cluster networks could describe the related icosahedral quasicrystals *i*-AlMnSi and *i*-AlCuLi (Henley, 1991b). A combination of 5 tetrahedra produces a pentagonal-bipyramid motif which is the basis for crystalline approximants [such as  $\text{Al}_{13}\text{Fe}_4$  and  $\text{T}_3(\text{AlMnZn})$ ] and for conjectured structure models of *decagonal* Al-transition metal quasicrystals (Henley, 1993). The corresponding combination in a Frank-Kasper structure [consisting of 5 truncated tetrahedra arranged around a central axis] is the “VF” cluster, a common motif in large-unit-cell Frank-Kasper alloys of simple metals (Samson, 1968; Samson, 1969). If we assume that such clusters are linked as in  $\text{Al}_{13}\text{Fe}_4$ , we produce a new hypothetical Frank-Kasper decagonal model *different* from the one presented in the present paper. (The “VF” motif is rarer in our models – it occurs only when five fat rhombi meet to form a star.) In the new structure model, the centers of neighboring clusters are separated by  $\tau a$  in the horizontal planes and by  $\pm c/2$  vertically. We have not observed or investigated such a model in simulations.

## 6.5 Beyond Two Dimensions

To describe real structures, we must go beyond static, perfectly stacked structures. The real structure has 2 extra dimensions: time, and the periodic direction  $z$ . Whether its ultimate state is random-tiling or a locked quasiperiodic tiling, a tiling can improve its order under annealing only by reshuffling of its tiles. For example, recognizing the fundamental reshuffling in the case of the binary tiling permitted an accelerated Monte Carlo move (Widom et al. 1987). Note that, although the tile rearrangement apparently involves a large volume, it is common that the reshuffling requires the motion of only a single atom (Widom and Phillips, 1993).

The problem of reshuffling has an obvious relation to that of stacking disorder: a realistic model must handle configurations in which the structure does not repeat precisely along the fivefold axis. Indeed, the structure as quenched was not strictly periodic in the stacking direction. Of course, such nonperiodicity may be considered a defect, and perhaps blamed on incomplete equilibration; however there are two senses in which it is necessary even in equilibrium.

First, reaching equilibrium usually demands some tile reshufflings. But in a 3D atomic structure based on a 2D tiling, every tile reshuffling requires rearranging an entire column of the atomic structure. Obviously this is easiest done one bit of the column at a time; the intermediate state is one with stacking randomness. Second, in the random-tiling explanation of the thermodynamic stability of quasicrystals, the contribution of tile-reshuffling entropy to the free energy is decisive; this entropy can be extensive only in an ensemble with stacking disorder (Henley, 1991a). Recently, Ritsch, Nissen, and Beeli (1995) have argued that common features in high-resolution transmission electron microscope images of  $d(\text{AlCoNi})$  are evidence of stacking randomness in this decagonal.

### 6.5.1 Reshuffling

The reshufflings in the case of the two-level tiling are simple and are shown in Fig. 9. We can trade off  $Q + S \leftrightarrow 2K$  (Fig. 9(a)) or  $Q + K \leftrightarrow K + Q$  (Fig. 9(b)), This reshuffling is the simplest fundamental move which can be used to visit from one state to another.

Local reshufflings of the T/R tiling are not possible; instead it is necessary to form a “defect tile” such as a skinny rhombus that is normally absent in that tiling. A defect tile can move through the tiling in what is called a “zipper move” (Oxborrow and Mihalkovič, 1995) since it leaves behind a rearranged structure.

One must check what reshufflings imply for the atoms. In particular, the number of each species ought to be conserved; otherwise the reshuffling is either blocked, or it creates substitutional defects, or it only takes place in a structure which is already substitutionally disordered in equilibrium.

In a rhombus tiling, the phason strain (which can be regarded as the deviation of the projection plane embedded in higher dimensional space from its ideal position) determines the number density of each kind of rhombus; since the rhombus content is conserved under reshuffling, so is the atomic content. The same thing is true in our T/R tiling, but not in the two-level (Q/K/S) tiling, because of the possibility of trading off  $Q + S \leftrightarrow 2K$ . (When divided into Penrose rhombi, both combinations have the same contents).

Indeed, our 2LT (Q/K/S) atomic structure model has serious problems with the reshufflings: the  $Q + S \leftrightarrow 2K$  reshuffling changes the content of the tiles from 29 L + 14 S to 28 L + 14 S, so one large atom disappears or has to become an interstitial. The  $Q + K \leftrightarrow K + Q$  reshuffling conserves the net atomic content of the tiles; however, the atomic rearrangement in which atoms jump the least distance would put atoms on the wrong site for their species. Simulations have shown that such substitutions are not acceptable; even a few of them destroy the stability of the structure. We have to admit that no better moves have been found up to now.

In a T/R tiling, the question of rearrangements is quite different since the only possible update move is a “zipper”, is an entire chain of tiles which closes on itself (Oxborrow and Mihalkovič, 1995), just as in triangle-square tilings (Oxborrow and Henley, 1993). Thus, the intermediate state

of a rearrangement involves not only stacking defects, but also defects within each layer (which would appear as special tiles other than T or R).

### 6.5.2 Stacking Randomness

In a nonperiodic stacking, we may presume the tilings describing adjacent layers are similar. Thus the spatial sequence of layers is much like the temporal sequence of a 2D tiling undergoing a series of reshufflings (Henley, 1991a). Each violation of periodicity presumably costs energy; most likely, one or two ways of doing so are less costly than any others, so it is a reasonable approximation to postulate as a *constraint* on the stacked tiling ensemble that layers can be related spatially only in such ways (point stacking defects). In the case of the Q/K/S tiling model, the obvious stacking defects are flips  $Q + S \leftrightarrow 2K$  and  $Q + K \leftrightarrow K + Q$  from one layer to the next. Since the positions of the atoms are similar in both states, these defects should be not too costly in energy.

An interesting experiment would be to create a stacking of layers from *completely different* 2D tilings, and see what structure it relaxes to. For the *dodecagonal* Frank-Kasper structure, in the monatomic case (Gähler and Roth, 1995), the atoms rearrange – while moving only short distances – until all the layers are *identical* and defect free; on the other hand, in the binary case of the same dodecagonal structure (L and S atoms, similar to the present paper) the structure cannot be healed with just short-distance moves; instead substitutional defects are introduced.

## Acknowledgments

J.R. would like to acknowledge a post doctoral fellowship from the DFG and the hospitality at Cornell University, Ithaca, where most of this work has been carried out. C.L.H. was supported by the U.S. D.O.E. grant DE-FG02ER89-45404.

## A Appendix: Inductive derivation of 2LT model

Here we describe the details of an alternate inductive path to the two-level tiling structure model of Sec. 3.3, using the typical structural features that emerged from our simulation (see Sec. 2). To start, take the fundamental motif to be the chains of icosahedra; let the quasilattice constant  $a$  be the spacing between motif centers. Adopt a zero-order description in which the pentagons in the chains are regular. In our simulation cell, the pentagons of these chains were linked by sharing edges in the B layer, but by sharing corners in the A layer; this requires the B layer pentagons to be smaller than the A layer pentagons. Specifically the pentagon radius (center to vertex) is  $\tau^{-1}a$  in the B layer, and  $a/2$  in the A layer.

To zero order, the small A pentagons should be S atoms and the large B pentagons should be L atoms. Placing these pentagons creates two kinds of too-close atom pairs, to be resolved either by combining two atoms into one or by relaxing them farther apart.

(i) In the B layer, whenever pentagon centers are separated by  $b$ , there will be a place (in a tile interior) where regular pentagon corners are separated by only  $\tau^{-1}$  of a pentagon edge, too short to be a valid interatomic distance. This occurs whenever two motifs are second neighbors on the tiling geometry, i.e. they are nearest neighbors to the same motif, forming an angle  $2\pi/5$  with it. These atoms relax perhaps 25% further apart from each other. These are the  $\gamma$  atoms and must become S atoms since they are obviously being squeezed.

(ii) In the A layer, the same pentagons whose centers are separated by  $b$  also have corners very close to each other – separated by  $(\tau^{-2}/2)a \approx 0.19a$ . In this case these sites should be merged, so that these are the  $\kappa, \lambda, \mu$  sites. Naturally, there is excess space near these sites so they should become L atoms.

## References

- Beeli, C., Nissen, H. U., and Robadey, J. (1991). *Phil. Mag. Lett.*, *63*, 87.
- Bergman, G., Waugh, J. L. T., and Pauling, L. (1957). *Acta Crystallogr.*, *10*, 254.
- Cockayne, E. (1994). *J. Phys. A*, *27*, 6107.
- Dzугutov, M. (1993). *Phys. Rev. Lett.*, *70*, 2924.
- Elser, V. and Henley, C. L. (1985). *Phys. Rev. Lett.*, *55*, 2883.
- Evans, D. J. and Morriss, G. P. (1983). *Chem. Phys.*, *77*, 63.
- Frank, F. C. and Kasper, J. S. (1958). *Acta Cryst.*, *11*, 184.
- Frank, F. C. and Kasper, J. S. (1959). *Acta Cryst.*, *12*, 483.
- Gähler, F. and Roth, J. (1995). In G. Chapuis and W. Paciorek (Eds.), *Aperiodic '94* (pp. 183). World Scientific, Singapore.
- Hausleitner, C. and Hafner, J. (1992). *Phys. Rev. B*, *45*, 115, 128.
- He, A. Q., Yang, Q. B., and Ye, H. (1990). *Philos. Mag. Lett.*, *61*, 69.
- Henley, C. L. (1986). *Phys. Rev. B*, *34*, 797.
- Henley, C. L. (1991a). In P. J. Steinhardt and D. P. DiVincenzo (Eds.), *Quasicrystals: the State of the Art*. World Scientific, Singapore.
- Henley, C. L. (1991b). *Phys. Rev. B*, *43*, 993.
- Henley, C. L. (1993). *J. Non-Cryst. Solids*, *153and154*, 172.
- Henley, C. L. and Elser, V. (1986). *Phil. Mag. B*, *53*, L59.
- Jeong, H.-C. and Steinhardt, P. J. (1994). *Phys. Rev. Lett.*, *73*, 1943.
- Katz, A. and Duneau, M. (1986). *J. Physique*, *47*, 181.
- Kreiner, G. and Franzen, H. F. (1995). *J. Alloys Compounds*, *221*, 15.
- Lançon, F. and Billard, L. (1990). *J. Phys. France*, *51*, 1099.
- Lançon, F., Billard, L., Burkov, S., and de Boissieu, M. (1994). *J. Physique France I*, *4*, 283.
- Lançon, F., Billard, L., and Chaudhari, P. (1986). *Europhys. Lett.*, *2*, 625.
- Li, X. Z. and Kuo, K. H. (1991). In K. H. Kuo and T. Ninomiya (Eds.), *Proceedings of China-Japan Seminars on Quasicrystals* (pp. 103). World Scientific, Singapore.
- Mihalkovič, M. (1995). In G. Chapuis and W. Paciorek (Eds.), *Aperiodic '94* (pp. 552). World Scientific, Singapore.
- Mihalkovič, M., Zhu, W.-J., Henley, C. L., and Oxborrow, M. (1996a). *Phys. Rev. B*, *53*, 9000.
- Mihalkovič, M., Zhu, W.-J., Henley, C. L., and Phillips, R. B. (1996b). *Phys. Rev. B*, *53*, 9021.
- Nissen, H.-U. and Beeli, C. (1993). *Int. J. Mod. Phys. B*, *7*, 1387.
- Oxborrow, M. and Henley, C. L. (1993). *Phys. Rev. B*, *48*, 6966.
- Oxborrow, M. and Mihalkovič, M. (1995). In G. Chapuis and W. Paciorek (Eds.), *Aperiodic '94* (pp. 178). World Scientific, Singapore.

- Phillips, R., Deng, H., Carlsson, A. E., and Murray, S. D. (1991). *Phys. Rev. Lett.*, *67*, 3128.
- Phillips, R., Zou, J., Carlsson, A. E., and Widom, M. (1994). *Phys. Rev. B*, *49*, 9322.
- Ritsch, S., Nissen, H.-U., and Beeli, C. (1995). In C. Janot and R. Mosseri (Eds.), *Proc. of the 5th Int. Conf. on Quasicrystals* (pp. 216). World Scientific, Singapore.
- Roth, J., Schilling, R., and Trebin, H.-R. (1990). *Phys. Rev. B*, *41*, 2735.
- Roth, J., Schilling, R., and Trebin, H.-R. (1995). *Phys. Rev. B*, *51*, 15833.
- Samson, S. (1968). In A. Rich and N. Davidson (Eds.), *Structural Chemistry and Molecular Biology* (pp. 687). W. H. Freeman, San Francisco.
- Samson, S. (1969). In B. C. Giessen (Ed.), *Developments in the Structural Chemistry of Alloy Phases*. Plenum, New York.
- Shoemaker, D. P. and Shoemaker, C. B. (1988). In M. V. Jarić (Ed.), *Introduction to Quasicrystals* (pp. 1). Academic Press, San Diego.
- Shoemaker, D. P., Shoemaker, C. B., and Wilson, F. C. (1957). *Acta Crystallogr.*, *10*, 1.
- Widom, M. and Phillips, R. (1993). *J. Non-Cryst. Solids*, *153and154*, 282.
- Widom, M., Phillips, R., Zou, J., and Carlsson, A. E. (1995). *Phil Mag B*, *71*, 397.
- Widom, M., Strandburg, K. J., and Swendsen, R. H. (1987). *Phys. Rev. Lett.*, *58*, 706.
- Zou, J. and Carlsson, A. E. (1994). *Phys. Rev. B*, *50*, 99.

layer	type	name	# in Q	# in K	# in S	# in 2T	# in 2R
X	S	$\alpha$	4	6	10	2	4
A	S	$\beta$	3	4	5	1	1
A	L	$\kappa$	0	1	0	0	0
A	L	$\lambda$	0	0	5	1	0
A	L	$\lambda'$	2	3	0	0	2
B	S	$\gamma$	0	0	5	1	1
B	S	$\gamma'$	0	2	0	0	0
B	S	$\delta$	2	2	0	0	2
B	L	$\mu$	2	3	5	1	0
B	L	$\mu'$	0	0	0	0	2
B	L	$\epsilon$	0	0	0	0	2

Table 1: Content of the tiles. First column: layer. Second column: type of atom. The labels are introduced in Figs. 4, 5. Third column: name of the site. Other columns: numbers in Q,K,S and T,R tiles.

layer	name	coord.	frequency
X	$\alpha$	12	$2(\tau + \tau^{-5})/\sqrt{5} = 1.52786$
A	$\beta$	12	$1 = 1.00000$
A	$\kappa$	15*	$\tau^{-5} = 0.09017$
A	$\lambda$	16	$\sqrt{5}\tau^{-5} = 0.20163$
A	$\lambda'$	15	$(2\tau + 3)/\tau^5 = 0.56231$
B	$\gamma$	12	$\sqrt{5}\tau^{-5} = 0.20163$
B	$\gamma'$	12*	$2\tau^{-5} = 0.18034$
B	$\delta$	14	$2(\sqrt{5} - 2) = 0.47214$
B	$\mu$	16	$(5 + \sqrt{5})\tau^{-5} = 0.65254$
X	$\alpha$	12	$2\tau = 3.23607$
A	$\beta$	12	$(3\tau-2)/2 = 1.42705$
A	$\epsilon$	14	$\tau^{-2} = 0.38197$
A	$\lambda$	16	$2\tau^{-1} = 1.23607$
A	$\lambda'$	15	$\tau^{-2} = 0.38197$
B	$\gamma$	12	$(3\tau-2)/2 = 1.42705$
B	$\delta$	14	$\tau^{-2} = 0.38197$
B	$\mu$	16	$2\tau^{-1} = 1.23607$
B	$\mu'$	15	$\tau^{-2} = 0.38197$

Table 2: Coordination polyhedra for the two level tiling (Q/K/S) and the triangle/rectangle (T/R) tiling. The fR/Q tiling can be derived from the T/R tiling by a subdivision of the tiles as indicated in Fig. 4. First column: layer (A,B,X). Second column: name of the site. The prime indicates a coordination number different from the standard. Third column: coordination number, the star indicates non-FK-coordination. Fourth column: relative frequency. The composition of the two level tiling is S:L = 0.692:0.382, the composition of the T/R tiling is S:L = 0.679:0.321.

Figure 1: Projection of the structure obtained by cooling down the ‘tenfold’ axis. Lines link neighboring chains of interpenetrating icosahedra and outline the tiles found in the structure. Four large circles outline the periodic boundary conditions. The two types of atoms are indicated by shape and size.

(a)

(b)

Figure 2: Rhombohedra with the Henley-Elser decoration; dark spheres are L atoms and light spheres are S atoms. Two cells are stacked above each other. The prisms are obtained by drawing new bonds (indicated by dashed lines). (a) Prolate rhombohedron transformed fat rhombic prism; (b) Oblate rhombohedron transformed a skinny rhombic prism.

(a)

(b)

Figure 3: Transformation of rhombic dodecahedron (RD) into decagonal Q tile. (a) The white spheres have to be removed. (b) After dividing into layers, the modified RD is reassembled into a hexagonal prism.

(a)

(b)

(c)

(d)

Figure 4: Basic tiles and basic decoration. The figures show a projection, with atoms marked by circles; atoms in A,B, and X layers are white,black, and centered circles respectively (see key); large (L) atoms are shown larger. Site classes are labeled by Greek letters. Dotted lines indicate the decomposition of the fat rhombus and Q tile into triangles and rectangles. (a) Fat Penrose tile (b) Skinny Penrose tile (c) Q tile. (d) Q tile in the fR/Q tiling. Light dashed lines divide it into three Penrose rhombi (used only for construction); dashed double lines show  $b$  edges, dividing it into a rectangle and two isosceles triangles. The “ $\delta$ ” atoms would be relaxed outwards in a more realistic model.

Figure 5: Decoration of the two-level tiling. Tile edges are shown solid; dashed edges show how they are combined from Penrose tiles.

Figure 6: Auxiliary tiling for the acceptance domains, topologically equivalent to the Q/K/S decoration, adapted to have integer coordinates. If the atoms on the large Penrose tile edges are shifted, the result is a deflated Penrose tiling but with varying decoration of the vertices. Long dashes: original tiles, short dashes: pentagon tiling, full and dashed lines indicate the small Penrose tiles.

Figure 7: Acceptance domain of the Q/K/S tiling. Here “ $z_{\perp}$ ” labels the commensurate component of perp-space. Greek letters show the atom class; the layer and species are indicated also. The symbols for the atoms are the same as in the other figures.

Figure 8: Truncated tetrahedron (solid lines) with  $\mu$  atom at center, showing its placement in the fat Penrose rhombus decoration. (The rhombus contains another truncated tetrahedron centered on a  $\lambda$  atom, which is not shown.)

a)

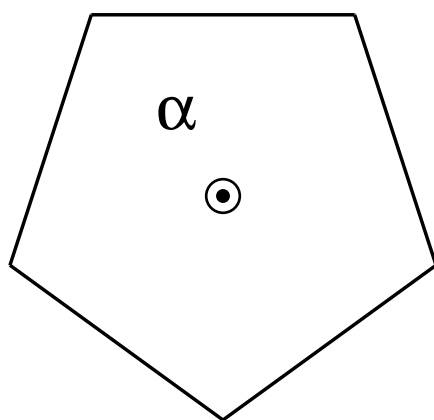
b)

Figure 9: Reshuffling operations in the two-level tiling. (a)  $Q + S \leftrightarrow 2K$  (b)  $Q + K \leftrightarrow K + Q$ . In each case, the dotted lines show the Penrose tiles into which the Q, K, and S tiles may be subdivided; both reshufflings correspond to the same reshuffling of the Penrose tiles.

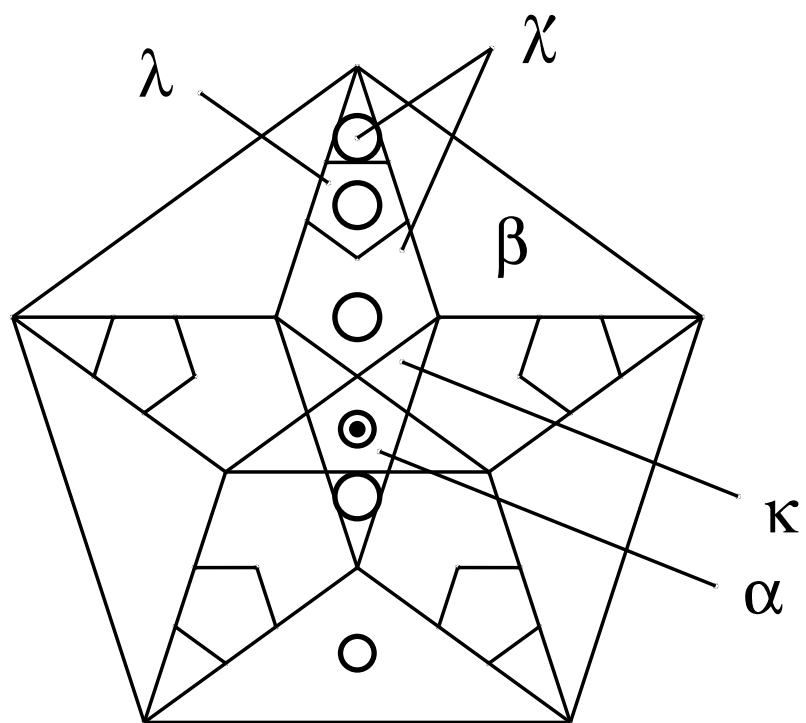
a)

b)

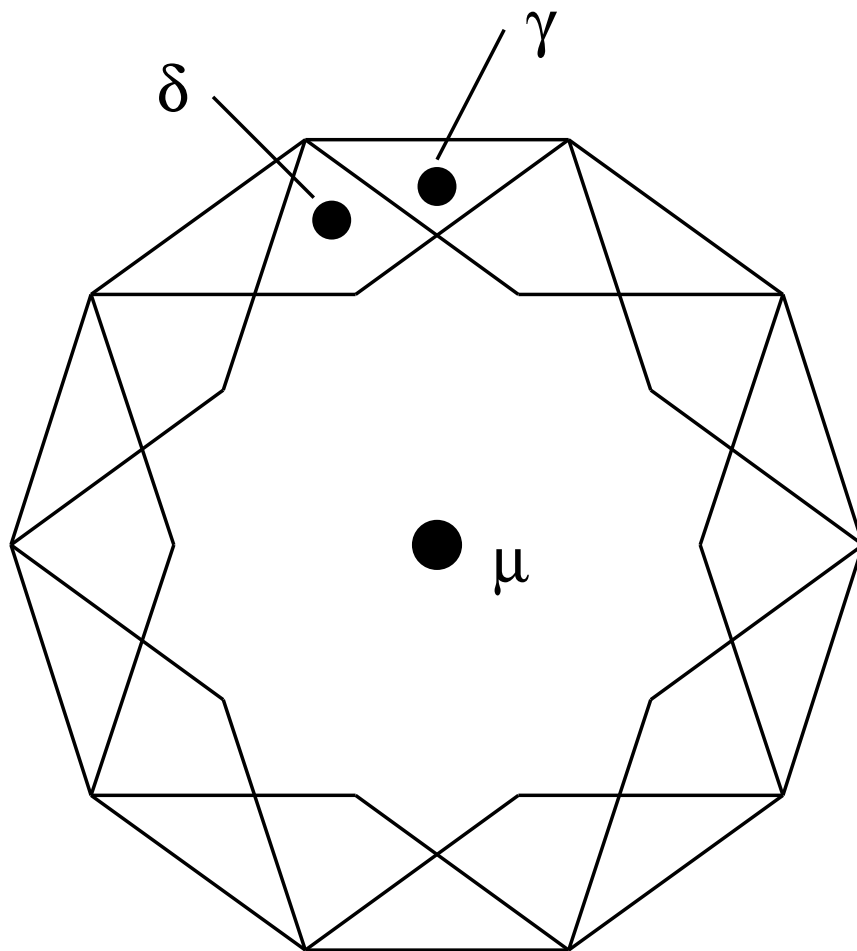
Figure 10: Thermodynamic properties from simulations with Dzugutov's potentials. (a) Potential energy *vs.* temperature at  $P = 0.1$  (b) Phase diagram for our binary decagonal quasicrystal. The sublimation line is shown solid. The crosses and plus signs indicate the actual simulation runs to determine the phase boundary. Note the absence of a liquid phase!



$$z_{\perp} = 0$$



$$z_{\perp} = 1$$



$$z_{\perp} = 2$$

